Particle Lithography from Colloidal Self-Assembly at Liquid−Liquid Interfaces

Lucio Isa,* Karthik Kumar, Mischa Müller, Jan Grolig, Marcus Textor, and Erik Reimhult

ETH Zürich, Laboratory for Surface Science and Technology, Wolfgang-Pauli-Strasse 10, 8093 Zürich, Switzerland

ARTICLE

ABSTRACT Particle lithography has been extensively used as a robust and cost-effective method to produce large-area, close-packed arrays of nanometer scale features. Many technological applications, including biosensing, require instead non-close-packed patterns in order to avoid cross-talk between the features. We present a simple, scalable, single-step particle lithography process that employs colloidal self-assembly at liquid−liquid interfaces (SALI) to fabricate regular, open particle lithography masks, where the size of the features (40 to 500 nm) and their separation can be independently controlled between 3 and 10 particle diameters. Finally we show how the process can be practically employed to produce diverse biosensing structures.

KEYWORDS: self-assembly · liquid interfaces · particle lithography · biosensing · colloidal lithography · nanoparticle monolayer · nanolithography

The growing need for miniaturization in diverse technological applications, such as biosensor arrays and biointerfaces, calls for rapid and cost-effective processing methods for the fabrication of regular structures controlled at the nanometer level over large areas. Particle lithography can respond to these needs[1] but traditional approaches lead to the formation of dense monolayers of colloidal spheres resulting in minimal separation between the fabricated features.[2−4] In optical and electrochemical sensing applications nanoscale features must be separated by many multiples of their size to avoid interfering responses, which presents a significant challenge. We demonstrate how colloidal self-assembly at liquid−liquid interfaces (SALI) can be used to deposit regular, open particle lithography masks which fulfill the requirements put forth above in a single-step process. We show that separations from 3 to 10 particle diameters for colloids ranging from 40 to 500 nm in diameter can be reproducibly achieved and applied to fabrication of diverse biosensor structures.

Particle lithography exploits the ability of colloidal particles to self-assemble into large-scale complex structures. Large-area, defect-free, close-packed crystalline assemblies of colloidal spheres have been successfully produced directly on solid substrates by means of controlled evaporation,[2] convective assembly,[3] spin-coating,[5] and electrophoretic deposition,[6,7] and have been used as lithography masks (positively, using the particles,[8] or negatively, using the interstitial spaces[5]). To achieve non-closed-packed assemblies one can follow several routes.[9] Colloids can be deposited directly from solution, either on plain or templated substrates. The former yields nonordered patterns and limited control on the particle separation,[4,10] while the latter offers accurate control on the final assembly but still requires expensive e-beam lithography to define the deposition template.[11,12] Alternatively, additional postprocessing steps of close-packed particle masks, e.g. etching, make it possible to achieve larger interfeature distances, albeit limited in choice of feature size-to-separation.[13,14] In contrast, oil−water interfaces are uniquely suited for the assembly of two-dimensional colloidal patterns unattainable by direct self-assembly at solid−liquid interfaces.[15] This is due to the combination of three key elements: (i) colloidal particles are strongly trapped at the interface yielding inherently two-dimensional structures;[16] (ii) particles retain lateral mobility within the interface despite the strong vertical trapping[17,18] and can therefore typically self-assemble into the minimum free energy configuration; and (iii) specific interactions arise between particles at the interface between polar and nonpolar immiscible fluids. In particular long-ranged electrostatic repulsion, stemming from charge imbalance at the interface, acts as the driving force to obtain the open crystalline structures we demonstrate in this paper.[19,20]

*Address correspondence to lucio.isa@mat.ethz.ch.

Received for review June 4, 2010 and accepted September 27, 2010.

Published online October 8, 2010.
10.1021/nn101260f

© 2010 American Chemical Society

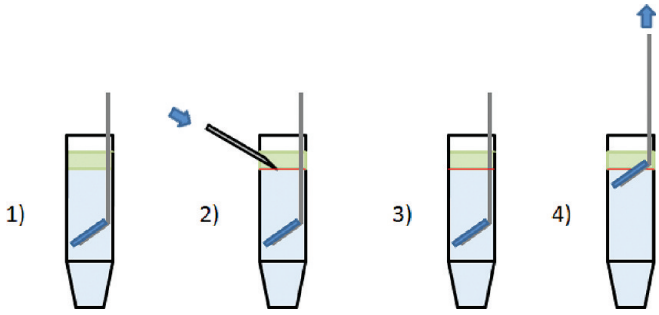

Figure 1. Schematics of the SALI particle deposition procedure: (1) substrate insertion and creation of the liquid−liquid interface, (2) particle injection at the interface, (3) equilibration, and (4) substrate extraction and pattern transfer.

In practical terms, forming a homogeneous pattern at the liquid interface is a crucial issue. This becomes increasingly challenging for smaller particles as electrostatic interactions become weaker. Homogenization is driven by diffusion and can be facilitated by injecting energy into the system, e.g. by subjecting the interface to compression/expansion cycles;[21] alternatively homogeneous patterns can be obtained by applying external electric fields.[22] After SALI, the particle pattern can be transferred onto a solid substrate and dried for further processing. The latter is often the most critical step in colloidal lithography during which an initially well-defined pattern can be disrupted. A first requirement to preserve the pattern upon transfer is to have strong adhesion between the particles and the substrate. This can be achieved, e.g., by creating an attractive electrostatic potential between colloids and substrates of opposite charge onto which the particles can be strongly bound by van der Waals forces upon adhesion. A second requirement is to ensure that capillary forces during drying of the fluid do not disrupt the pattern; this is more critical for larger (micrometer-sized) colloids due to greater drag. Capillary forces can also be reduced, e.g., by solvent exchange prior to drying.[23]

RESULTS AND DISCUSSION

We describe a general procedure to use SALI to create non-close-packed patterns on the true nanometer scale with unprecedented control on the feature spacing. Moreover, compared to previous demonstrations, our method does not require delicate solvent exchange procedures,[23] it minimizes the requirements for substrate modification and does not necessitate external action (e.g., compression cycles).[21] Our approach is demonstrated at water/hexane interfaces for positively charged amidine latex particles of diameters (D) ranging from 40 to 500 nm, with subsequent transfer to a variety of silicon-based solid substrates. Moreover, we show through quantitative analysis of microscopy images that the interparticle separation, or nearest neighbor distance (d) can be tuned by controlling the concentration of particles at the interface and that the obtained results follow a simple prediction for regular particle arrangements. These advances turn SALI into a versatile, low-cost, parallel lithographic technique for creation of regular patterns over the large areas and parameter space of nanoscale feature sizes and separations necessary in many sensor and biointerface applications.

The processing steps for SALI lithography are the following (see Figure 1). A clean, *hydrophilic* (water contact angle 20−30°), negatively charged silicon oxide or nitride substrate is positioned horizontally onto a holder with a tilt angle of ~10° and then inserted into the water phase. The nonpolar phase (*n*-hexane, 10 mL) is poured on top of the water to create the liquid−liquid interface. A suspension of positively charged particles (amidine polystyrene beads) is injected directly at the interface with a needle connected to a high precision peristaltic pump. The particles are suspended in a mixture of water and isopropanol, which acts as spreading solvent;[24] after injection, the particles are irreversibly trapped at the interface.[16] By construction of the liquid cell, the fluid interface has a fixed cross-sectional area. The area density of the particles and therefore their separation is thus controlled by the amount of particles injected at the interface N_p, leading to smaller d for more crowded interfaces. We point out that curvature effects of the interface do not play a major role given that typical substrates are significantly smaller (1 cm^2) than the liquid−liquid interfacial area (4.5 cm^2) and that they are placed in the center of the cell where the meniscus is practically flat. However, we emphasize that the cross-sectional area of the cell and hence the area of substrate that can be patterned are scalable with no inherent limitations. The particles are positively charged and hydrophobic (we measured directly a contact angle of 110(±3)° for the 500 nm particles and assume hydrophobic character for all particle sizes; see the Supporting Information for further details); the former is required to provide adhesion onto the substrate and the latter ensures that they protrude into the oil phase through which the long-range electrostatic repulsion required for the formation of open ordered arrangements is mainly mediated.[20,25] The system is left equilibrating for a particle size-dependent time (see the Supporting Information for details) followed by the extraction of the substrate using a linear motion driver at a speed of 25 μm/s to collect the colloids by sweeping through the interface. A hydrophilic substrate ensures that the wetting by the oil happens slowly and only through a well-defined meniscus when going from the aqueous to the nonpolar phase. The substrate dries as it emerges from the oil phase into the air and, as mentioned previously, this last drying step is crucial for the pattern transfer as even the strong adhesion of the positively charged particles to the substrate can be overcome by capillary forces and viscous drag. We believe that the choice of the right solvent has been one of the hinder-

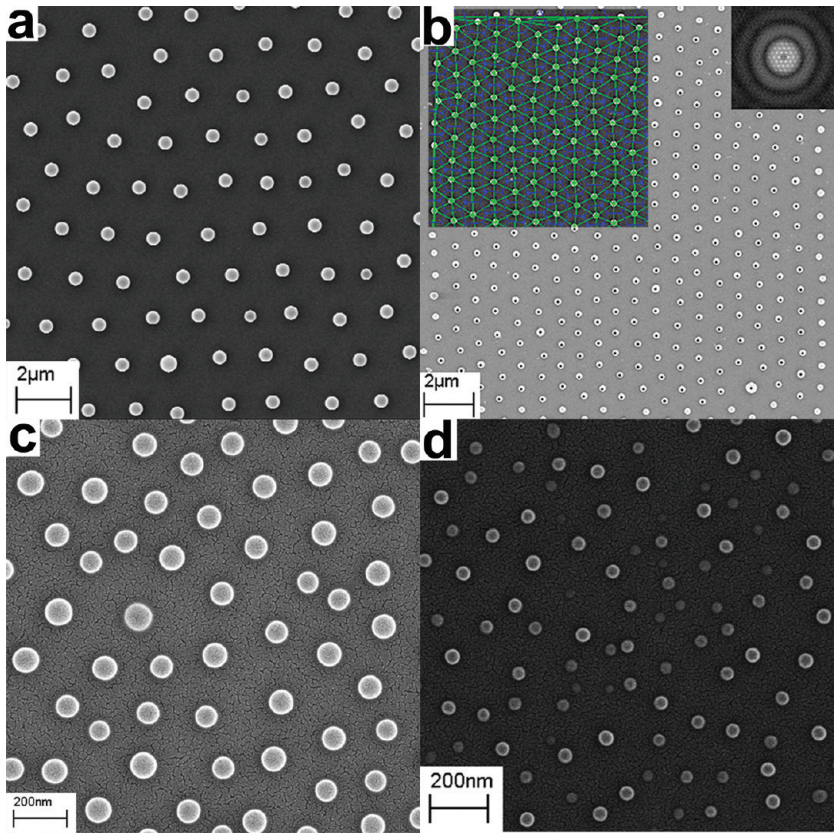

Figure 2. SEM images of (a) 500, (b) 200, (c) 100, and (d) 40 nm in average diameter amidine latex polystyrene particles deposited on SiO_2. (b) Superimposed to the particles, we show the outcome of the locating algorithm, with Delaunay particle triangulation (green) and Voronoi areas (blue) highlighted in the upper left corner. In the bottom right corner we see how a larger particle distorts the lattice. Inset upper right: FFT of the image demonstrating the long-range spatial order.

ing points in previous attempts to use SALI for particle depositions and we found that hexane offers the right characteristics in terms of low viscosity and high volatility to allow for seamless transfer. Investigations on the use of different alkane solvents are reported in the Supporting Information; however, we point out that the requirement becomes less stringent for smaller particles for which the viscous drag of the drying solvent is lower.

The method is also very flexible in terms of the use of different substrates, with the sole requirements that they are oppositely charged compared to the particles and hydrophilic. Our approach can thus also be applied with negatively charged nanoparticles by reversing the charge of the substrate through coating with a polyelectrolyte layer (e.g., PDDA, ACH, *etc.*) as already shown for random sequential colloid adsorption.[4,10]

Examples of the outcome of the SALI deposition are reported in Figure 2. An example of the quantitative image analysis is reported in Figure 2b. Each of the particles in the image is identified (as shown by the cross hair) *via* an image analysis algorithm. The original SEM image is overlaid in the top left corner with a triangulation that connects all the particle centers (Delaunay triangulation) and with the Voronoi polygon construction that highlights the available area per particle.[26] By reducing the particle size from 500 to 40 nm we observe that the regularity of the arrangement decreases (see Figure 2c/d). This can be attributed to several reasons, including the fact that the smaller latex particles have larger polydispersity and the fact that Brownian motion has for smaller sizes a stronger effect in displacing the particles from the minimum of the electrostatic potential well. This, on average, larger relative displacement will be frozen in at the moment of transfer. For 500 and 200 nm particles we obtained polycrystalline monolayers, with a typical domain size of tens of μm^2 within which long-range order is found. The main advantage of SALI as opposed to direct deposition of particles from solution is that, even in the absence of long-range order, as for the smallest colloids, short-range order is always present over a large concentration range; this means that particles are never aggregated and that we are always able to define a preferred nearest neighbor distance d. From the particle location algorithm[27,28] we extract particle coordinates with high accuracy (typically <5 (SEM) and <20 nm (optical)) (see the Supporting Information). The coordinates were used to compute the radial distribution function ($g(r)$) and from it extract d, as the position of the first peak. Figure 3a shows three examples of the radial distribution functions. The first case (red curve) shows optimal SALI deposition; long-range order is noticeable from the presence of several well-defined peaks in $g(r)$ corresponding to the preferred nearest,

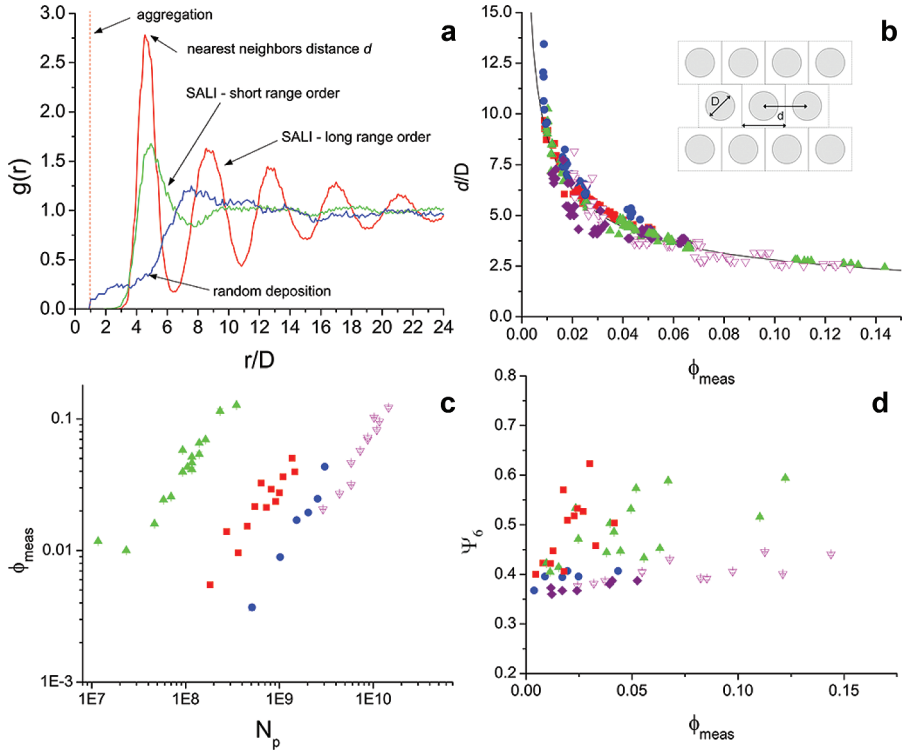

Figure 3. (a) Examples of radial distribution functions: long-range order SALI (red), short-range order SALI (green), and random sequential deposition (blue). The vertical dashed line highlights the distance for particle aggregation; in both SALI cases we report complete absence of aggregation. (b) Normalized nearest neighbor distance *d* as a function of the local particle area fraction ϕ_{meas}. Inset: Schematics of the modeling for calculating the prediction on the functional dependence of the *d* versus local area fraction. A completely random assembly yields no scaling. (c) "Calibration curves" which show local measured area fraction versus the deposited number of particles N_p. Error bars have the same size of the symbols and indicate variation in ϕ_{meas} over the entire substrate (1 cm^2). (d) Order parameter Φ_6 versus local area fraction. We observe an increase for higher concentrations. Φ_6 is 1 for a perfect hexagonal crystal. In all graphs: (▲) 500 nm, (■) 200 nm, (●) 150 nm, (▽) 100 nm, and (♦) 40 nm.

second, third, *etc.* neighbor distances. We then highlight a second case of non-optimal SALI (green curve), where long-range order is absent, but short-range order is still present with a well-defined *d*. Moreover, we notice how in both cases, $g(r)$ drops sharply to zero well before $r = D$, which corresponds to undesired particle contacts in the deposited pattern. A completely different outcome is depicted by the blue curve, which relates to the case of random sequential adsorption directly on the solid substrate. In this case, we note both the absence of a well-defined *d* and the occurrence of particle aggregation (see the Supporting Information for details).

Assuming an ordered array, the images can be tessellated by square tiles whose size corresponds to the center-to-center distance. Under this assumption the interparticle distance scales with local area fraction Φ_{meas} following $d/D = [\pi/(4\Phi_{meas})]^{1/2}$. Figure 3b shows that the experimental data are in strong agreement with this prediction and that separations can be well controlled at least in the interval from 3 up to 10 particle diameters. The observed scaling is not trivial; it is the consequence of well-defined short-range order. Completely random particle patterns and the presence of aggregation will void such description. The local particle density, and thus *d*, can be controlled externally by tuning the number of particles added to the interface (Figure 3c); the error bars in the graph and the spread of the data points estimate the long spatial wavelength variations in the local density across cm^2 sized substrates, which could be due to slow convection at the liquid interface prior and during transfer. The only exception are the 40 nm particle samples for which the local relation between Φ_{meas} and *d* still holds but for which larger inhomogeneities over the substrate are present making it more difficult to achieve predictive control over *d*. Finally, we observe that the degree of long-range order depends on the particle concentration at the interface. Figure 3d shows the values of the order parameter Φ_6 as a function of Φ_{meas}; this parameter is 1 for a perfect hexagonal lattice. Increasing particle concentration increases order due to that stronger interactions occur between particles at shorter distances.

In biosensing the inherent statistical nature of data collected by addressing single structures and the sampling of a large number of structures by near- or far-field probes requires both regular positioning and large separations. The advantages of SALI for lithographic patterning are thus particularly clear for applications in, e.g., optical, nanoplasmonic, and electrochemical

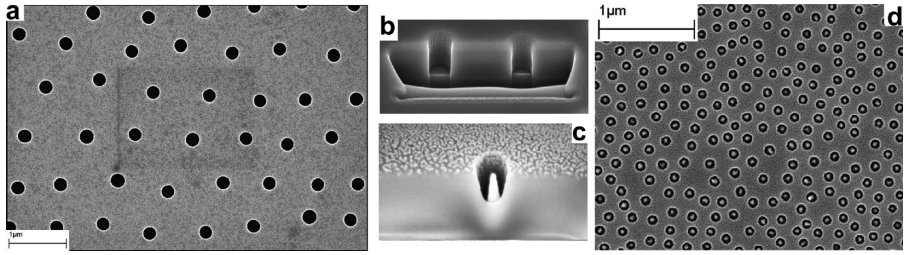

Figure 4. (a) SEM image of nanoplasmonic 200 nm hole array in a 40 nm thick Ti/Au film. (b) Focused ion beam (FIB)-SEM side view of 200 nm wide nanopores in a 300 nm thick silicon nitride on a silicon wafer. We note that the side walls are etched straight throughout the nitride layer and that the etching stops at the silicon surface. (c) FIB-SEM side view of a gold nanocone inside a 100 nm diameter pore etched into a 240 nm thick silicon nitride film. (d) SEM view of nanocone array with aspect ratio 1:1 deposited into 100 nm pores. We note the presence of a gold nanocone in each nanopore grown from the bottom of the pore and extending to the outer surface.

biosensing. Three such sensor substrate examples produced by SALI are shown in Figure 4 for ordered nanoplasmonic hole arrays, non-cross-talking electrochemical nanopore electrodes, and arrays of SERS-active Au nanocones embedded in a silicon nitride film. To produce these structures SALI patterns of latex particles were deposited as a lift-off mask for evaporation of a Ti/Au film for structure in Figure 4a[8] and for evaporating a Cr etch mask for subsequent reactive ion etching (RIE) for the structures in Figure 4b and c/d.[10] Lift-off of the particles by tape stripping after the Ti/Au film evaporation results in the plasmonic sensor substrate in Figure 4a. The nanopore substrate in Figure 4b is obtained by wet removal of the Cr mask after RIE. Finally, the nanocone SERS active substrate in Figure 4c/d is obtained after an additional evaporation of a thick Au film onto the pore structure in Figure 4b before Cr mask removal.[8] Lift-off of the Cr layer results in the pore-localized Au cones with a height determined by the thickness of the evaporated Au layer.

In summary, we have reported a general method for the deposition of non-close-packed regular arrays of colloidal nanoparticles through self-assembly at liquid−liquid interfaces, allowing both feature (particle) size and spacing to be controlled *independently* within a large range. The interparticle distance was controlled by changing the area fraction of the particles injected at the interface. Importantly, we showed that by deposition through a low-viscosity, high-volatility solvent the particle pattern could be transferred unperturbed to the solid substrate. The simple control of particle order and spacing by the electrostatic interaction of particles inserted at the interface at a controlled density suggests interesting extensions of the work in terms of depositing higher order patterns. As can be seen in Figure 2b larger colloids change the local spacing and this effect is predicted to lead to a large number of different nontrivial patterns for binary size mixtures.[29,30]

While demonstrated here for colloidal lithography using amidine polystyrene particles to produce patterns of interest for ongoing biosensor projects within our group, we emphasize the generality of the method in terms of particle and substrate materials, substrate size, and even nonplanar shapes, and finally we point out that SALI is applicable to any of the many process variations which use particle masks described in the literature.[1,8]

METHODS

Materials. We used amidine polystyrene particles from Invitrogen/Interfacial Dynamics Corporation (see the Supporting Information for more details). Prior to injection at the interface, the batch particle solutions (4% w/v) were diluted appropriately in a 6:4 Milli-Q water ($R = 18.2\ \Omega$, TAC < 6 ppb):isopropanol (gradient grade for liquid chromatography, Merck, Germany) solution. The interfaces were created between Milli-Q water and *n*-hexane (UV spectroscopy grade, Sigma-Aldrich, USA) in polypropylene 50 mL centrifuge tubes (TPP, Switzerland). The particle patterns were deposited on silicon substrates, either untreated or coated with layers of silicon oxide or nitride. The coated chips were either fabricated in house with Plasma Enhanced Chemical Vapor Deposition or obtained as a gift from Leister Process Technologies (Switzerland). Prior to use, the substrates were cleaned *via* successive ultrasonication in toluene (HPLC grade, Acros Organic, USA), isopropanol, and Milli-Q water (each step for 30 min). Static water contact angles were measured on each substrate batch prior to use.

Imaging. Images of deposited patterns have been obtained both *via* optical and scanning electron microscopy. In the former we used an upright microscope (model Nikon Eclipse L200) in reflection mode with magnifications of ×50 and ×100−×150 for 500 and 200 nm particles respectively, allowing for the imaging of areas ranging from 50000 to 5000 μm^2. SEM (Zeiss Ultra 55) was used for the 40, 100, and 150 nm particles and for high-resolution images of 200 and 500 nm colloids. Prior to imaging, the samples were sputter-coated with 3−5 nm of platinum to avoid charging. Details of the quantitative image analysis are given in the Supporting Information. The side view of the nanopores was obtained with a SEM-FIB Zeiss NVision 40.

Fabrication of the Nanoporous Substrates and the SERS Nanocones. After deposition of the particles, 20−30 nm of metallic Cr was evaporated onto the surfaces at a rate of 2 Å s^{-1} (Univex 500, Oerlikon Leybold Systems). All metals for evaporation (Au, Ti, Cr) were obtained from Unaxis (Switzerland). Particles were then stripped with scotch tape and subsequently sonicated in pure acetone and Milli-Q water, using the Neytech Ultrasonik Cleaner 104H-W, for at least 30 min each. Using the metallic Cr as an etch mask, straight-walled pores were anisotropically etched in a Plasmalab 80+ RIE II etcher (Oxford Instruments), using a gas mixture of 50 sccm CHF_3 and 5 sccm O_2 for 20 min at nominal power of 70 W and a chamber pressure of 10 mTorr. To fabricate the

nanocones we subsequently evaporated 2 nm Ti at 2 Å s^{-1} and 120 nm Au at 2 Å s^{-1} onto the etched substrates. The shadowing effect of buildup of Au at the top of the pores, decreasing the effective pore size with increased Au thickness, yields the observed conical structures. Finally, the Cr mask, and thereby the Au covering the top surface, was removed by using a Balzers liquid chrome etch. Pores with diameters ranging between 40 nm and 5 μm with depths of up to 1 μm were reproducibly achieved. Nanocones with base diameters ranging between 100 and 200 nm and heights between 100 and 300 nm were also achieved with this technique.

Acknowledgment. The authors acknowledge FP7-NMP-ASMENA and Swiss NCCR nanoscale science for funding. Leister Process Technologies are acknowledged for providing substrates. ETH Zurich nanofabrication center FIRST and its staff, R. Wepf, and ETH Zurich centre for electron microscopy (EMEZ) are acknowledged for support.

Supporting Information Available: Additional details and information relative to the materials (particles, contact angle measurements) and processes (effects of equilibration times and solvents, comparison with random sequential deposition, and details on the quantitative image analysis) described in the paper. This material is available free of charge via the Internet at http://pubs.acs.org.

REFERENCES AND NOTES

1. Velev, O. D.; Gupta, S. Materials Fabricated by Micro- and Nanoparticle Assembly - The Challenging Path from Science to Engineering. *Adv. Mater.* **2009**, *21*, 1897–1905.
2. Denkov, N. D. et al. Mechanism of Formation of 2-Dimensional Crystals from Latex-Particles on Substrates. *Langmuir* **1992**, *8*, 3183–3190.
3. Dimitrov, A. S.; Nagayama, K. Continuous Convective Assembling of Fine Particles into Two-Dimensional Arrays on Solid Surfaces. *Langmuir* **1996**, *12*, 1303–1311.
4. Hanarp, P.; Sutherland, D. S.; Gold, J.; Kasemo, B. Control of Nanoparticle Film Structure for Colloidal Lithography. *Colloids Surf., A* **2003**, *214*, 23–36.
5. Hulteen, J. C.; Vanduyne, R. P. Nanosphere lithography - A Materials General Fabrication Process for Periodic Particle Array Surfaces. *J. Vac. Sci. Technol., A* **1995**, *13*, 1553–1558.
6. Lumsdon, S. O.; Kaler, E. W.; Williams, J. P.; Velev, O. D. Dielectrophoretic Assembly of Oriented and Switchable Two-Dimensional Photonic Crystals. *Appl. Phys. Lett.* **2003**, *82*, 949–951.
7. Zhang, K. Q.; Liu, X. Y. In Situ Observation of Colloidal Monolayer Nucleation Driven by an Alternating Electric Field. *Nature* **2004**, *429*, 739–743.
8. Fredriksson, H. et al. Hole-Mask Colloidal Lithography. *Adv. Mater.* **2007**, *19*, 4297–4302.
9. Jiang, P.; Prasad, T.; McFarland, M. J.; Colvin, V. L. Two-Dimensional Non Close-Packed Colloidal Crystals Formed by Spincoating. *Appl. Phys. Lett.* **2006**, *89*, 011908.
10. Reimhult, E.; Kumar, K.; Knoll, W. Fabrication of Nanoporous Silicon Nitride and Silicon Oxide Films of Controlled Size and Porosity for Combined Electrochemical and Waveguide Measurements. *Nanotechnology* **2007**, *18*, 275303.
11. Yin, Y. D.; Lu, Y.; Gates, B.; Xia, Y. N. Template-Assisted Self-Assembly: A Practical Route to Complex Aggregates of Monodispersed Colloids with Well-Defined Sizes, Shapes, and Structures. *J. Am. Chem. Soc.* **2001**, *123*, 8718–8729.
12. Kraus, T. et al. Nanoparticle Printing with Single-Particle Resolution. *Nat. Nanotechnol.* **2007**, *2*, 570–576.
13. Blattler, T. M. et al. From Particle Self-Assembly to Functionalized Sub-Micron Protein Patterns. *Nanotechnology* **2008**, *19*, 075301.
14. Plettl, A. et al. Non-Close-Packed Crystals from Self-Assembled Polystyrene Spheres by Isotropic Plasma Etching: Adding Flexibility to Colloid Lithography. *Adv. Funct. Mater* **2009**, *19*, 3279–3284.
15. Binks, B. S.; Horozov, T. S. *Colloidal Particles at Liquid Interfaces*; Cambridge University Press: Cambridge, UK, 2006.
16. Binks, B. P.; Lumsdon, S. O. Influence of Particle Wettability on the Type and Stability of Surfactant-Free emulsions. *Langmuir* **2000**, *16*, 8622–8631.
17. Wu, J.; Dai, L. L. Apparent Microrheology of Oil−Water Interfaces by Single-Particle Tracking. *Langmuir* **2007**, *23*, 4324–4331.
18. Dhar, P.; Prasad, V.; Weeks, E. R.; Bohlein, T.; Fischer, T. M. Immersion of Charged Nanoparticles in a Salt Solution/Air Interface. *J. Phys. Chem. B* **2008**, *112*, 9565–9567.
19. Pieranski, P. Two-Dimesional Interfacial Colloidal Crystals. *Phys. Rev. Lett.* **1980**, *45*, 569–572.
20. Bresme, F.; Oettel, M. Nanoparticles at Fluid Interfaces. *J. Phys.: Condens. Matter* **2007**, *17*, 413101.
21. Ray, M. A. et al. Submicrometer Surface Patterning Using Interfacial Colloidal Particle Self-Assembly. *Langmuir* **2009**, *25*, 7265–7270.
22. Aubry, N.; Singh, P.; Janjua, M.; Nudurupati, S. Micro- and Nanoparticles Self-Assembly for Virtually Defect-Free, Adjustable Monolayers. *Proc. Natl. Acad. Sci. U.S.A.* **2008**, *105*, 3711–3714.
23. Ray, M. A.; Jia, L. Micropatterning by Non-Densely Packed Interfacial Colloidal Crystals. *Adv. Mater.* **2007**, *19*, 2020–2022.
24. Reynaert, S.; Moldenaers, P.; Vermant, J. Control over Colloidal Aggregation in Monolayers of Latex Particles at the Oil−Water Interface. *Langmuir* **2006**, *22*, 4936–4945.
25. Horozov, T. S.; Aveyard, R.; Binks, B. P.; Clint, J. H. Structure and Stability of Silica Particle Monolayers at Horizontal and Vertical Octane−Water Interfaces. *Langmuir* **2005**, *21*, 7405–7412.
26. Preparata, F. P.; Shamos, M. I. *Computational Geometry: An Introduction*; Springer Verlag: New York, 1993.
27. Crocker, J. C.; Grier, D. G. Methods of Digital Video Microscopy for Colloidal Studies. *J. Colloid Interface Sci.* **1996**, *179*, 298–310.
28. Besseling, R.; Isa, L.; Weeks, E. R.; Poon, W. C. K. Quantitative Imaging of Colloidal Flows. *Adv. Colloid Interface Sci.* **2009**, *146*, 1–17.
29. Fornleitner, J.; Lo Verso, F.; Kahl, G.; Likos, C. N. Ordering in Two-Dimensional Dipolar Mixtures. *Langmuir* **2009**, *25*, 7836–7846.
30. Ebert, F.; Keim, P.; Maret, G. Local Crystalline Order in a 2D Colloidal Glass Former. *Eur. Phys. J. E: Soft Matter Biol. Phys.* **2008**, *26*, 161–168.